Electronic Supplementary Material (ESI) for Green Chemistry.
This journal is © The Royal Society of Chemistry 2023

Supplementary Information

Green Hydrogen Generation Assisted by Electroreforming of Raw Sugarcane Bagasse Waste

Li Quan Lee, Hu Zhao, Tian Yee Lim, Ge Junyu, Ovi Lian Ding, Wen Liu, and Hong Li

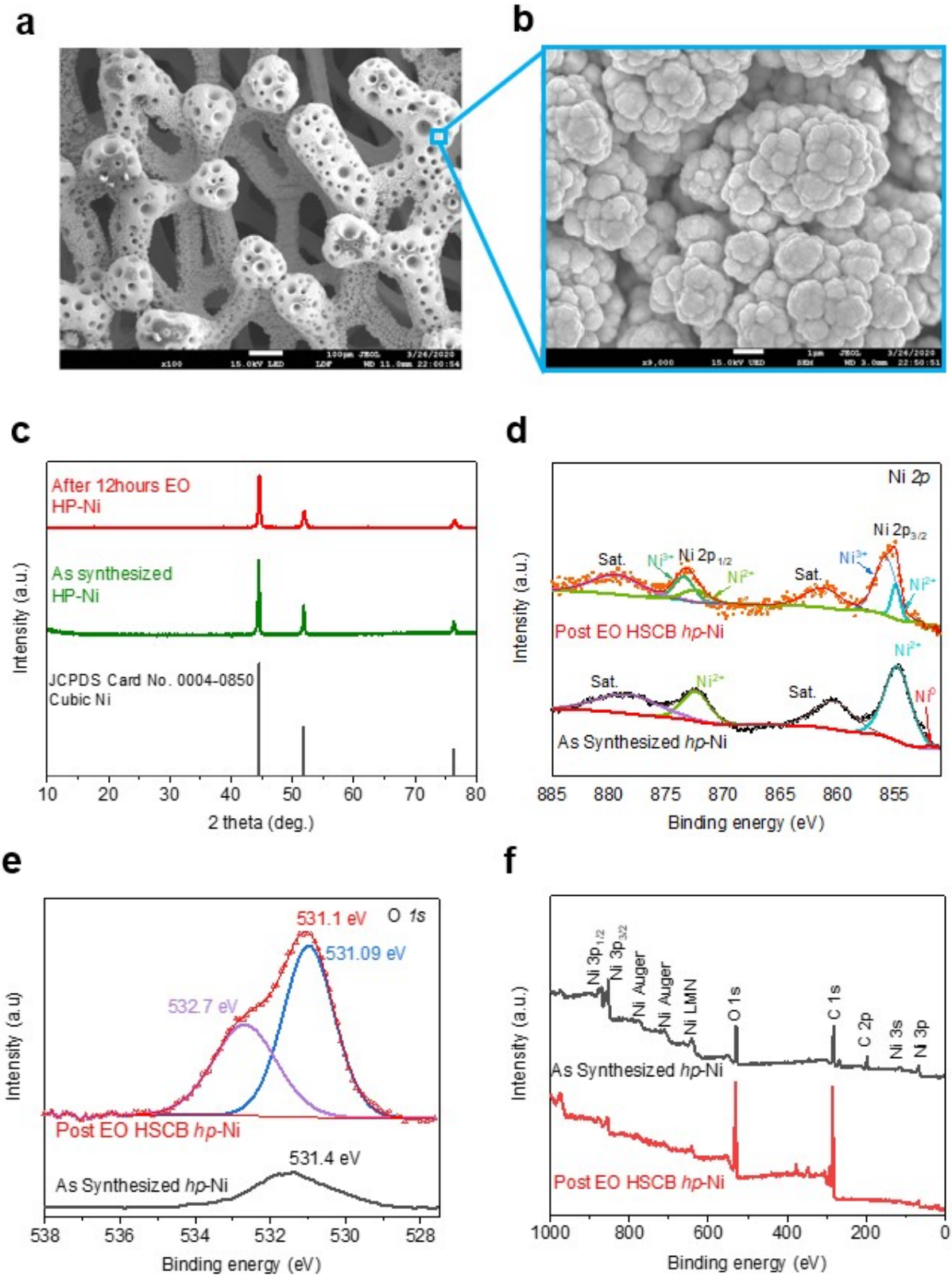

Figure S1: *hp*-Ni - a) SEM image, b) zoom-in SEM image of region at (a); c) XRD of *hp*-Ni - *After 12hours EO* (electrooxidation) of glucose (red spectra), *As Synthesized* (green spectra) and cubic Ni standard from JCPDS card No. 0004-0850(black spectra). XPS spectra of d) Ni *2p* states, e) O *1s* state, and f) full survey spectra of *As Synthesized hp*-Ni electrode after activation (black spectra) and *Post EO HSCB* for 4hrs at 1.58 V vs RHE (red spectra)

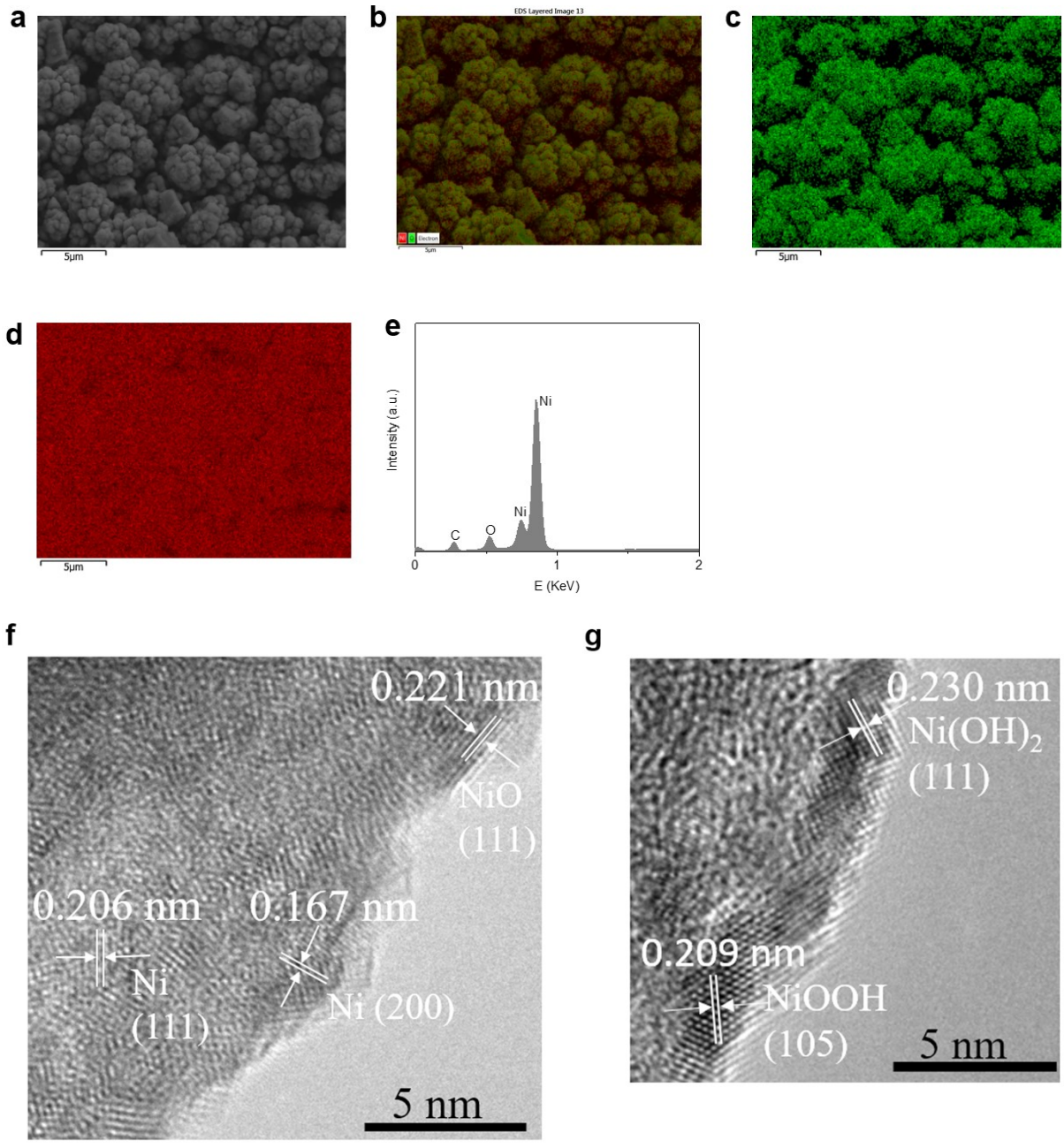

Figure S2: *hp*-Ni - a) SEM image used for EDS analysis; *hp*-Ni EDS - b) combined layered image of the detected elements, c) oxygen element mapping image, d) nickel element mapping image, e) EDS spectrum of area in image (a). HR-TEM images of nanoparticles from f) As Synthesized *hp*-Ni, showing the d-spacing of 0.206 and 0.167 nm of fcc Ni (111) and (200) planes, respectively. The d-spacing of 0.221nm corresponds to NiO (111) plane; g) Post EO HSCB *hp*-Ni, showing the d-spacing of 0.209 and 0.230 nm of NiOOH (105) and $Ni(OH)_2$ (111) planes, respectively.

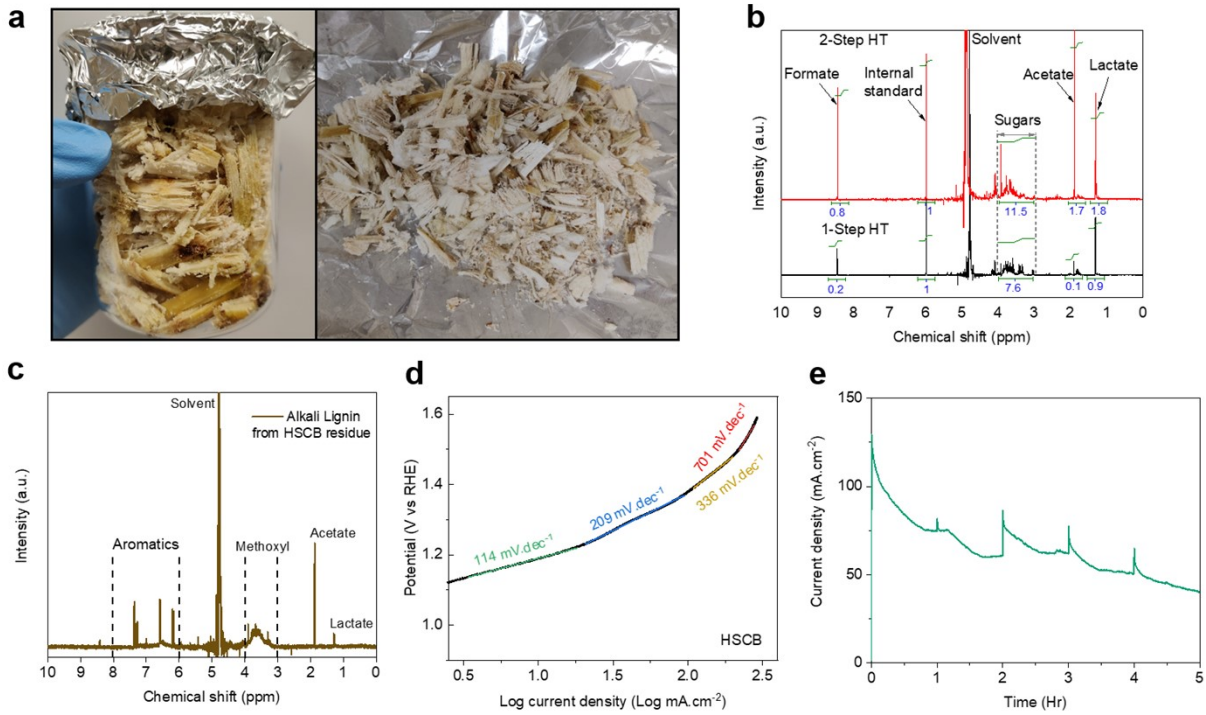

Figure S3: Raw sugarcane bagasse processing – a) RSCB rough cut to smaller pieces (Left: Before dry, Right: after overnight drying) b) ^{1}H NMR spectrums of RSCB after dilute H_2SO_4 hydrothermal process (Black: 1-Step Hydrothermal (HT), Red: 2-Step HT) with maleic acid as internal standard; c) ^{1}H NMR spectrum of dissolved products from residue of HSCB by mild alkaline treatment; d) Tafel plot derived from a current–potential curve obtained of *hp*-Ni electrode at scan rate 5 mV.s^{-1} of HSCB e) Chronoamperometric plot of HSCB electrooxidation in 1M KOH at constant potential at 1.58V vs RHE for 5hours

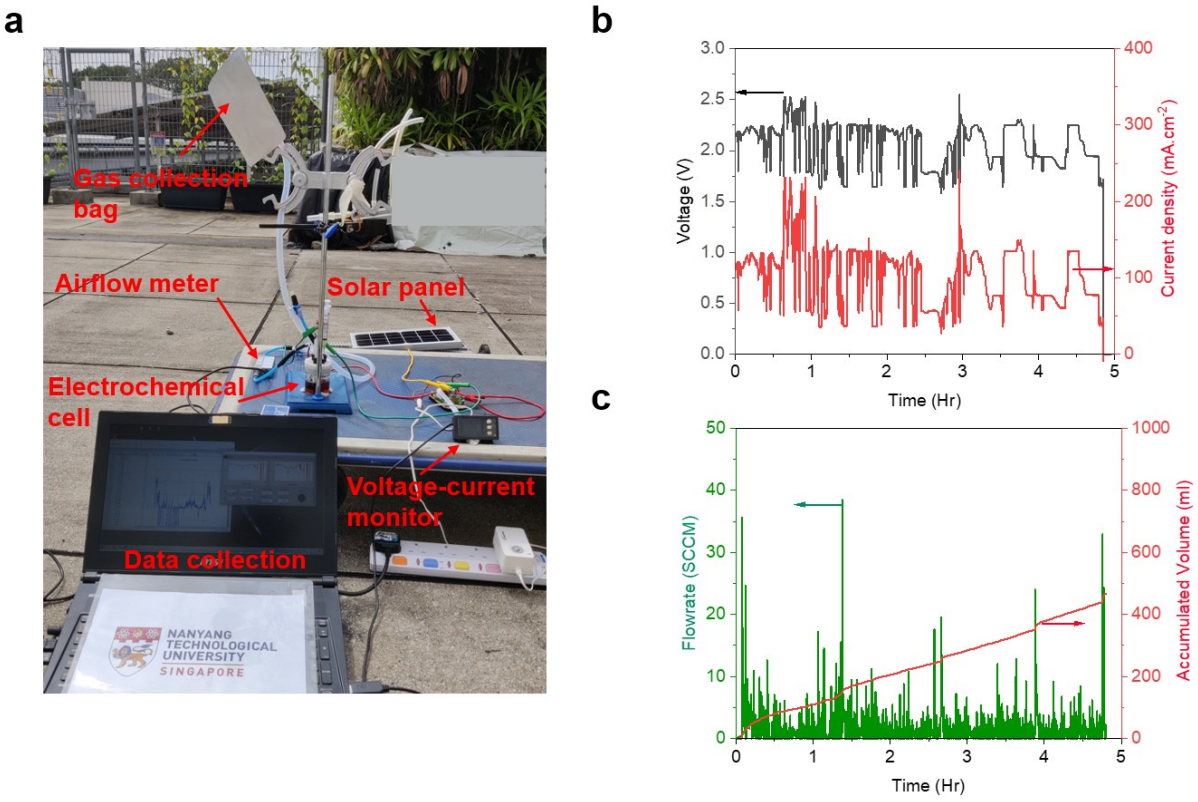

Figure S4: Solar-driven electroreforming of HSCB - a) Experimental setup; Real-time monitoring of b) Voltage with Current density; c) Gas flow rate with accumulated volume

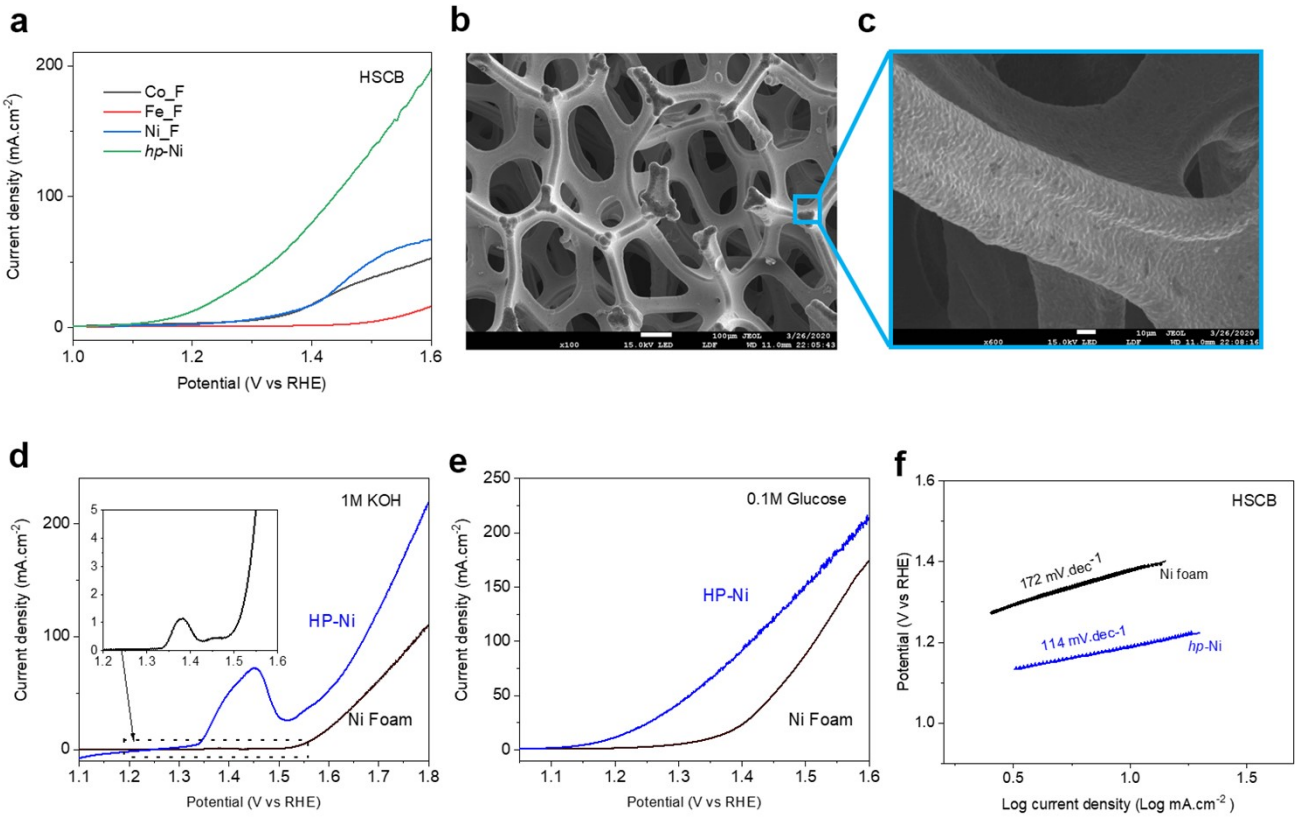

Figure S5: a) LSV of nickel foam (Ni-F), cobalt foam (Co-F), iron foam (Fe-F) and *hp*-Ni in HSCB. Bare Ni Foam – b) SEM image, c) zoom-in SEM image of region in image (b); LSV of Bare NF (black curve) vs *hp*-Ni (blue curve) - d) in 1M KOH e) with addition of 0.1M Glucose, and f) their corresponding Tafel slopes in HSCB

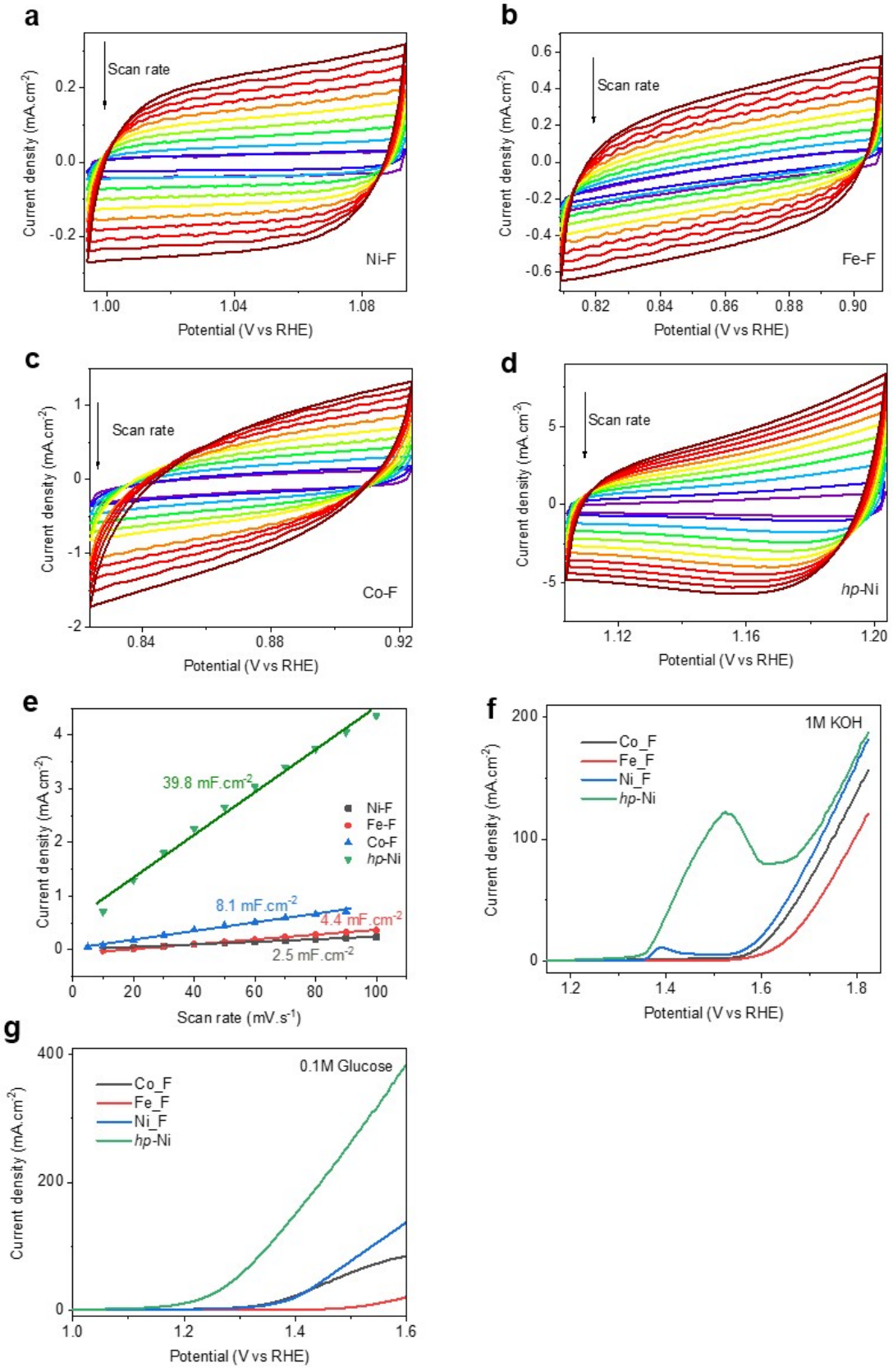

Figure S6: Electrochemical active surface area (ECSA) measurements. CV curves of - a) Ni-F, b) Fe-F, c) Co-F, and d) hp-Ni collected in 1.0 M KOH solution at the non-Faradaic region with different scan rates. e) Linear-fitted scan rate dependence of the current density difference at the open circuit potential; LSV of Co-F, Fe-F and Ni-F and hp-Ni as working anode in - f) 1.0 M KOH solution, g) 0.1M Glucose in 1.0M KOH solution.

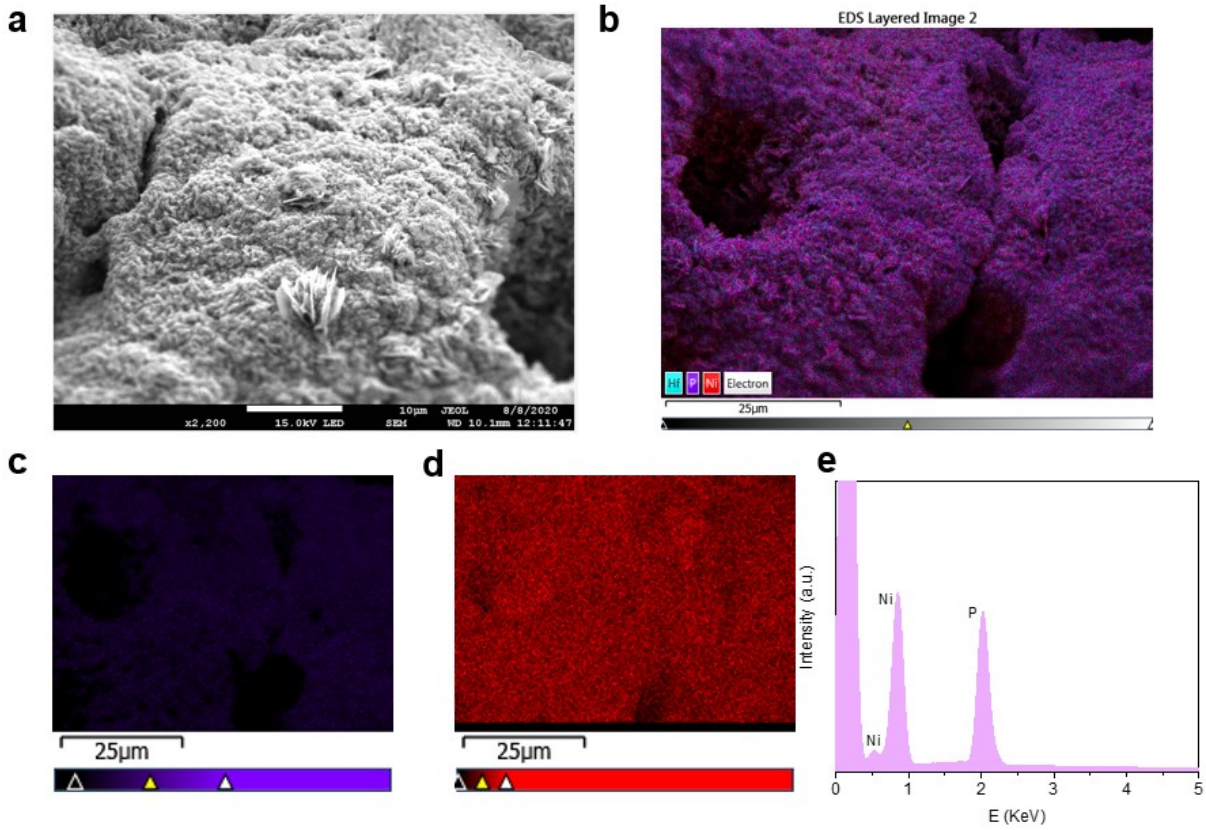

Figure S7: Ni_2P/Ni-F cathode - a) SEM image; Ni_2P EDS - b) combined layered image of the detected elements, c) phosphorus element mapping image, d) nickel element mapping image, e) EDS spectrum of area in image (a)

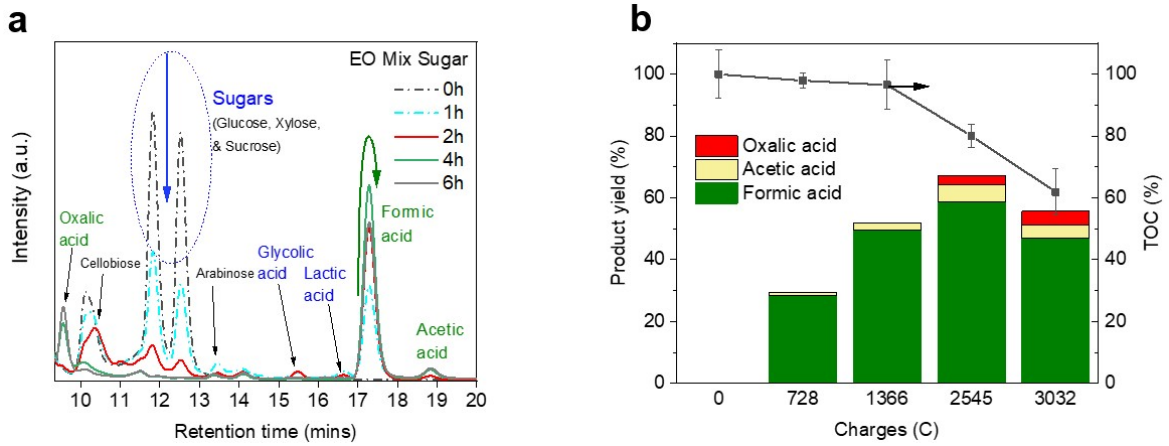

Figure S8: Electrooxidation of mixture of various saccharides (carbon mole ratio of 35% glucose, 10% cellobiose, 35% xylose and 20% sucrose), a) HPLC chromatograms at different intervals at 1.58V vs RHE and b) Effect of charges on product analysis (oxalic acid, acetic acid and formic acid)

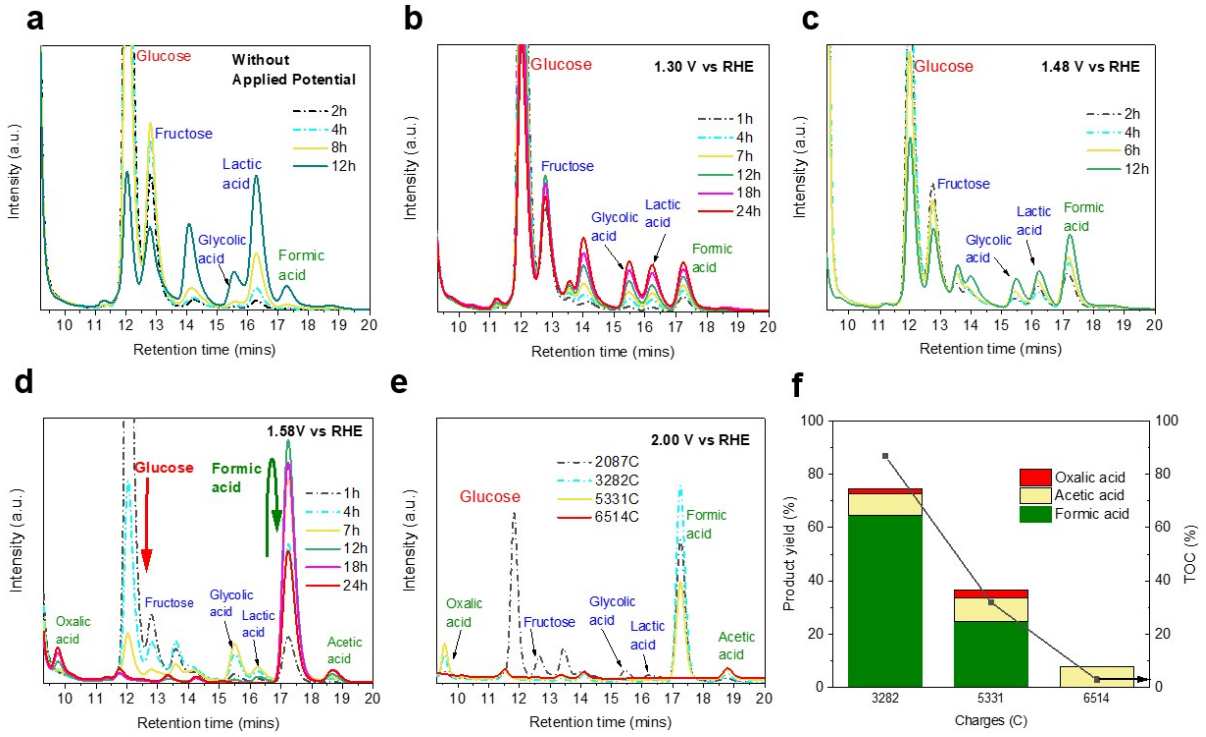

Figure S9: HPLC chromatograms of glucose electrooxidation at – a) 0V vs RHE, b)1.30V vs RHE, c)1.48V vs RHE, d) 1.58V vs RHE, e) 2.00V vs RHE; f) Effect of applied charges on products yield% (oxalic acid, acetic acid and formic acid) and TOC % from electrooxidation of 0.1M Glucose at 2V vs RHE.

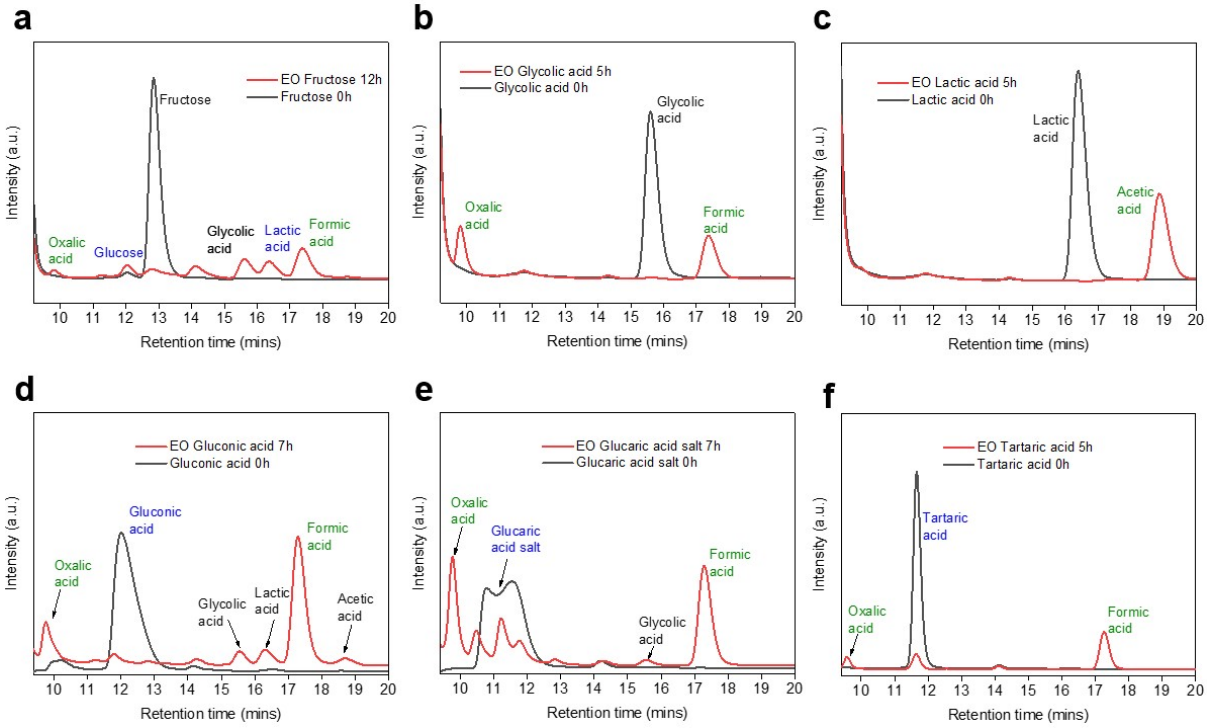

Figure S10: Electrooxidation of Intermediates – a) Fructose; b) Glycolic acid; c) Lactic acid; and electrooxidation of possible intermediates - d) Gluconic acid; e) Glucaric acid salt; f) Tartaric acid

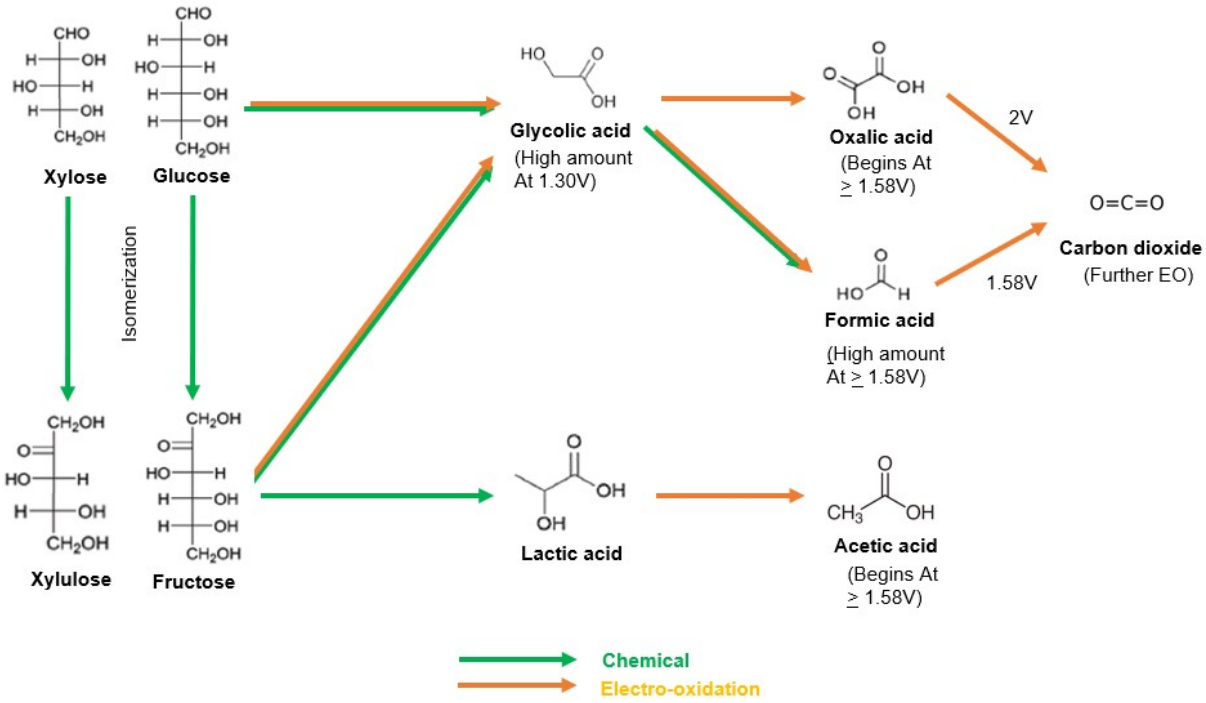

Figure S11: Proposed reaction pathway of xylose / glucose to formic acid, and other products.

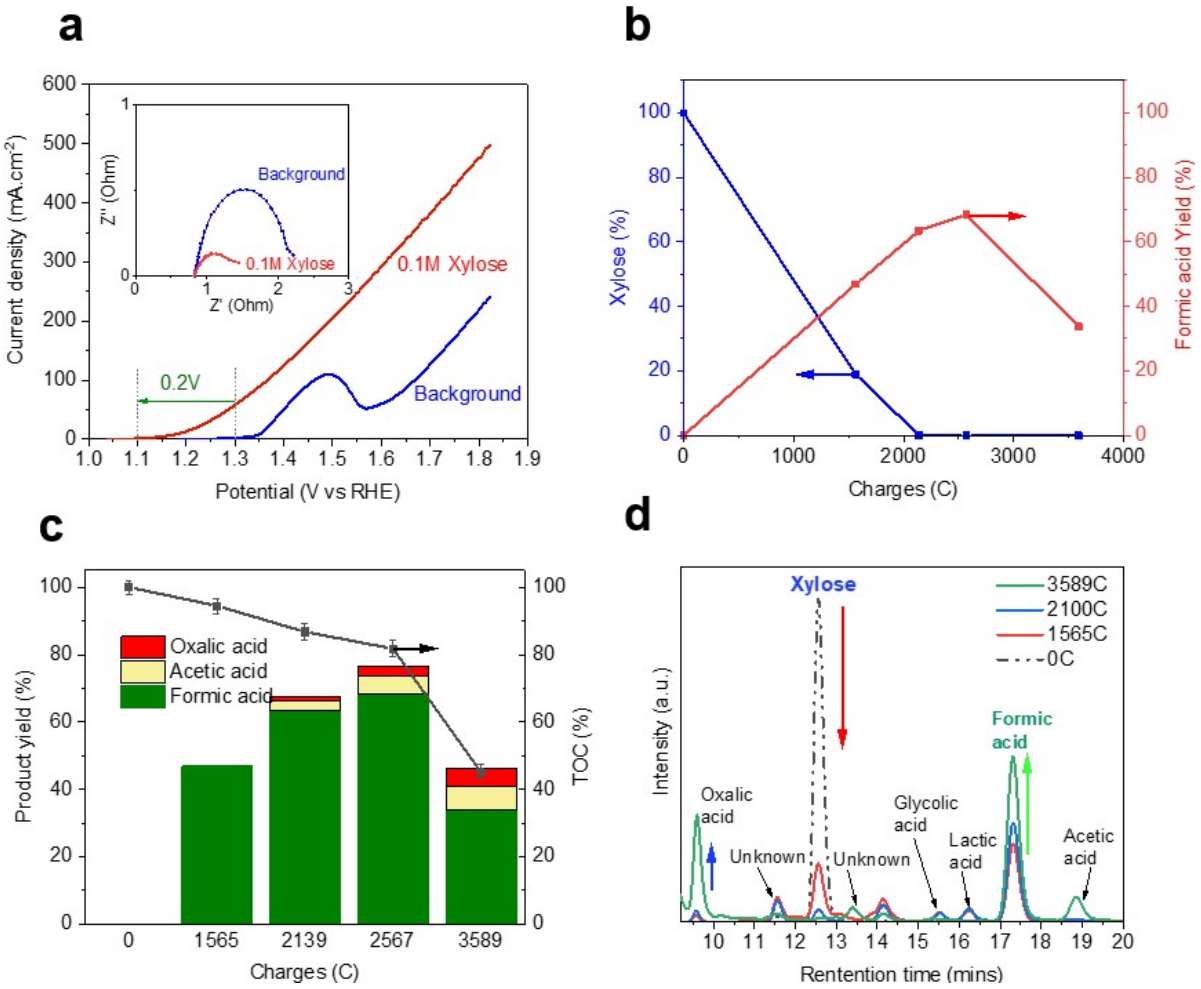

Figure S12: Xylose electrooxidation tests a) LSV of *hp*-Ni working anode (blue curve: background 1M KOH, red curve: 0.1M glucose in 1M KOH), Inset: Nyquist plots in 1M KOH at 1.58V vs. RHE; b) Effect of charges on formic acid yield % and xylose conversion% at 1.58V vs. RHE; c) Effect of charges on product analysis (oxalic acid, acetic acid and formic acid) and TOC % from electrooxidation of 0.1M xylose at 1.58V vs RHE; d) HPLC chromatograms of xylose electrooxidation at 1.58V vs RHE

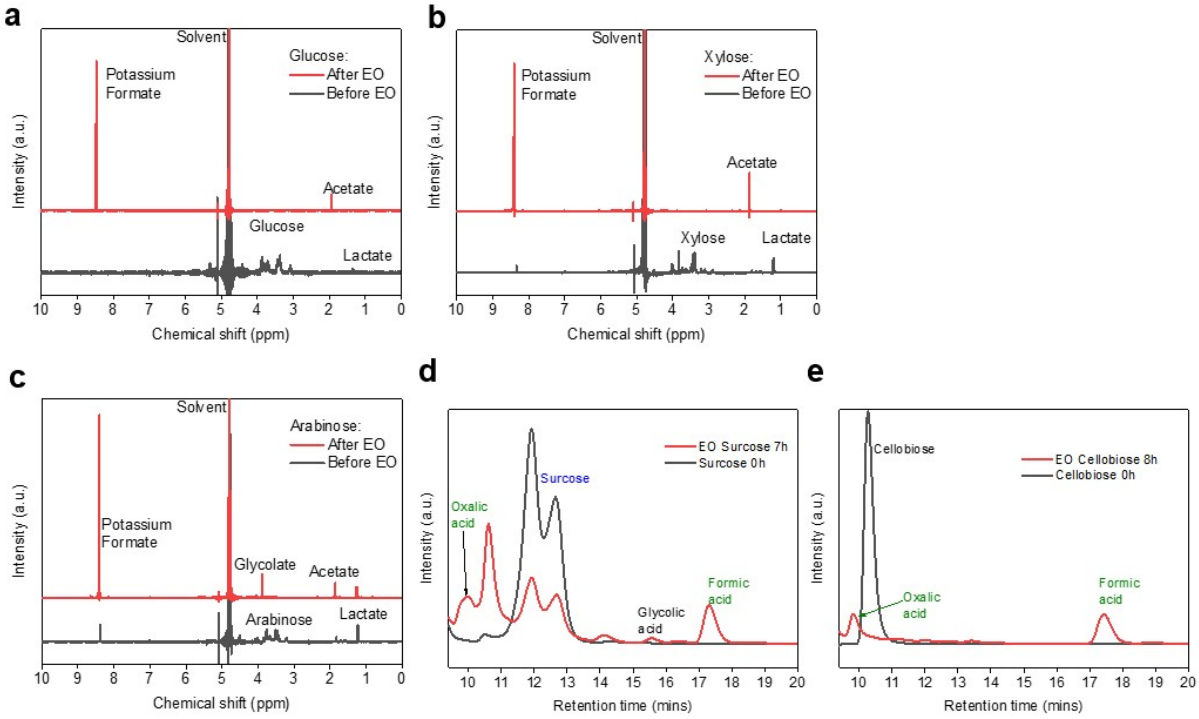

Figure S13: ^{1}H NMR spectrums of before and after electrooxidation of monosaccharaides - a) glucose; b) xylose; c) arabinose (Black curve: Before electrooxidation, red curve: After electrooxidation); and HPLC chromatograms of before and after electrooxidation of disaccharides – d) sucrose; e) cellobiose

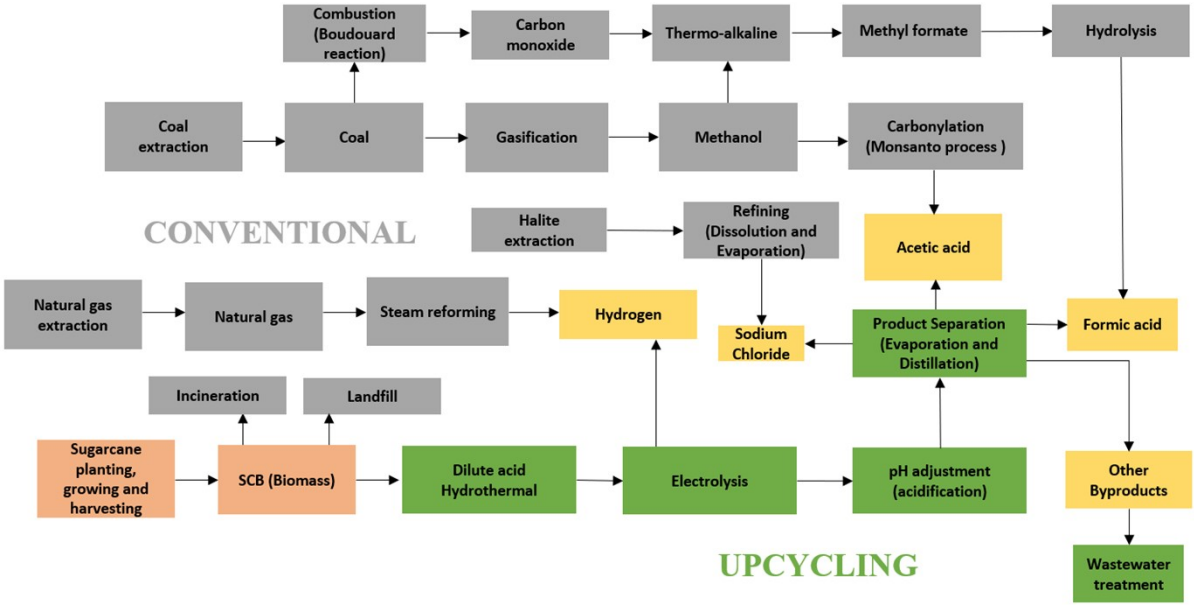

Figure S14: The process systems of (1) conventional waste treatment and (2) electro-upcycling of SCB waste, considered by a cradle-to-gate life cycle assessment for the present work, showing (grey) the conventional and (green) the novel upcycling routes. The products (yellow) considered include formic acid, acetic acid, sodium chloride, hydrogen, and other byproducts.

Table S1
Utilities used and their corresponding global warming potential assumed in LCA.

Utility	Electricity from natural gas [1]	Electricity from photovoltaic [1]	Process steam from natural gas [1]	Process steam from biomass [1]	Heat from municipal waste incineration [2]	Cooling water via cooling tower [3]
Global warming potential (kg CO_2-eq/kWh)	0.469	0.0322	0.253	0.014	0.000779	0.00264

Table S2
Sugarcane bagasse composition. [4]

Component	**wt.%**
Hemicellulose	27
Lignin	23
Cellulose	46
Ash	4

Table S3
Elemental composition, in oxides basis, of SCB ash. [5]

Chemicals	wt.%
SiO_2	54.9
Al_2O_3	7.8
CaO	4.9
Fe_2O_3	10
SO_3	1.2
MgO	2.5
K_2O	3
Na_2O	0.2
Others	3.2
Loss on Ignition (LOI)	12.2

Table S4
Flow inventory of the SCB upcycling process, as modelled in LCA. LCA data source [1] and [2] refer to Sphera database and Ecoinvent 3.8 database, respectively.

Flows	Amount	LCA data source
Input		
Cane bagasse	1000 kg	(2)
Sulphuric acid	94 kg	(1)
Process water	162 kg	(1)
Sodium hydroxide	2006 kg	(1)
Hydrochloric acid	1479 kg	(1)
Sulfolane	138 kg	(1)
Electricity	6925 kWh	(1)
Heating	8190 kWh	(1)
Cooling	8144 kWh	(3)
Output		
Hydrogen, H_2	39 kg	(1)
Formic Acid (>99%)	366 kg	(1)
Acetic Acid (>99%)	86 kg	(1)
Sodium chloride	2371 kg	(1)
Carbon dioxide	34 kg	(1)
Wastewater	1983 kg	(2)

Table S5
Anodic oxidation of Lignocellulosic biomass

Anodic oxidation (Lignocellulosic biomass)	Electrode	Current density	Product selectivity	Stability	Ref.
Black liquor	Pt, Ni and AISI 304 Stainless steel	< 10 $mA.cm^{-2}$	No product analysis	N. D	(6)
Kraft lignin	Pt, Au, Ni, Cu, DSA-O_2 and PbO_2	< 3 $mA.cm^{-2}$	<17% selectivity to Vanillin	N. D	(7)
Cellulose	Glassy carbon plates	0.2 to 0.4 mA	No specific product	N. D	(8)
Cellulose & Cellobiose	Gold	< 2 $mA.cm^{-2}$	No product analysis	N. D	(9)
Cellulose, Oligosaccharides	MnO_2/graphite/PTFE	< 5 $mA.cm^{-2}$	High selectivity to glucose	N. D (24h)	(10)
Cellulose	Gold	< 1 $mA.cm^{-2}$	No product analysis	N. D	(11)
Hemicellulose	Gold	< 1 $mA.cm^{-2}$	No product analysis	N. D	(12)
Lignin	Ni/C, Co/C, NiCo/C	< 5 $mA.cm^{-2}$	No specific product	N. D (2h)	(13)
Cellulose	AuNPs/C	< 1 $mA.cm^{-2}$	No product analysis	N. D	(14)
Cellulose	Au/carbon aerogel	10mA at 2.75Vcell	67.8% Gluconate	N. D (24h)	(15)
Lignin derivatives	PtFe/C	208 $mA.cm^{-2}$	90% CO_2	N. D (1.1h)	(16)
Lignin	Pt-Ru catalyst	< 4 $mA.cm^{-2}$	No product analysis	10 CV cycles (0 to 1.1V_{cell})	(17)
Lignocellulose mono- and Disaccharide derivatives	PtFe/C	0.15–0.2 $mA.cm^{-2}$	Near 100% selectivity to CO2	N. D (1.1h)	(18)
Lignin and its model compounds	Glassy carbon (GC)	25-80 mA	No specific product	N. D (24h)	(19)
Crushed barley straw	Nickel foam	< 3 $mA.cm^{-2}$	No specific product	80h	(20)
Glucose	Nickel	3.9 $mA.cm^{-2}$	22% Formate, 12% Oxalate, 7% Glycolate and 8% carbonates	N. D (6h)	(21)
Xylose	Nickel	3.9 $mA.cm^{-2}$	42% Formate, 5% Oxalate, 16% Glycolate and 7% carbonates	N. D (6h)	(21)
Sugarcane bagasse	*hp*-Ni	Average 100 $mA.cm^{-2}$	41% Formate, 9% Oxalate, 13% Acetate	3 CA runs (5 hours each)	This work
Glucose	*hp*-Ni	Average 216 $mA.cm^{-2}$	88% Formate, 0.5% Oxalate, 9% Acetate	3 CA runs (5 hours each)	This work
Xylose	*hp*-Ni	Average 170	68% Formate,	3 CA runs	This

		mA.cm^{-2}	3% Oxalate, 5% Acetate	(5 hours each)	work

N.D denotes no details. CA denotes Chronoamperometry. CV denotes Cyclic Voltammetry.

Table S6 Energy efficiency comparison of AWE and HSCB electro-reforming

Parameters	**AWE**	**HSCB electroreforming**
Electricity consumed	203 MJ	178 MJ
Energy of H_2 generated	142 MJ	142 MJ
Energy efficiency	70%	80%

Based on 1kg H_2 produced, which requires 33.8kg of SCB. HHV for the combustion of hydrogen is 285.8 kJ/mole. (22)

Supplementary Notes 1

For the life cycle assessment (LCA), the system boundary, as shown in Figure S12, starts from the sugarcane plantation, which also accounts for upstream activities. After retrieval of the by-product of the sugarcane plantation, i.e. sugarcane bagasse from cane sugar production, the processing of sugarcane bagasse includes extraction, electrolysis, and product separation. The resulting products are further purified by multi-evaporators, neutralisation, and distillation. The parameters used to model the separation process in the multi-evaporators is based on the relative molar solubility of the resulting salts, e.g. chlorides, acetates and formates. Here, the temperature and water content of the process streams are moderated to effectively recycle the solvent and separate formate and acetate salts. By-products such oxalate, sulphate and carbonate salts leave the system in a separate stream, which is sent for wastewater treatment. After this salt separation, hydrochloric acid is introduced to neutralise the remaining base and displace the weak organic acids (e.g. formic and acetic acid) from the salts. The displaced acids are evaporated for further purification e.g. by distillation. The distillation process uses sulfolane entrainer to achieve separation of the water-formic acid-acetic acid azeotropic mixture.[23] Three distillation columns were set up in series in order to extract water, then formic acid, and acetic acid sequentially.

Supplementary Notes 2

The energy efficiency calculation (22) is based on the heating value of produced hydrogen gas with respect to required energy consumed by the system as follows equation:

$$\eta_{eff} = \frac{HHV_{H2\ produced}}{Electricity\ consumed}\ X\ 100\%$$

where $HHV_{H2\ produced}$ is the higher heating value of the produced 1Kg of hydrogen (142 MJ), and *Electricity consumed* is the input energy for the water electrolysis or our electroreforming process. At a current density of 200 mA.cm^{-2}, the potential of AWE and HSCB electroreforming is 1.8 V vs RHE and 1.58 V vs RHE, respectively, suggesting a 12% higher efficiency.

Table S6 compares the energy efficiency of our HSCB electroreforming process and AWE.

References

1. Sphera Solutions GmbH, GaBi LCA Database Documentation. 2022 [Available from: https://gabi.sphera.com/databases/gabi-data-search/.
2. Wernet G, Bauer C, Steubing B, Reinhard J, Moreno-Ruiz E, Weidema B. The ecoinvent database version 3 (part I): overview and methodology. The International Journal of Life Cycle Assessment. 2016;21:1218-30.
3. Schulze C, Thiede S, Herrmann C. Life cycle assessment of industrial cooling towers. Progress in Life Cycle Assessment. 2019:135-46.
4. Pippo WA, Luengo CA, Alberteris LAM, Garzone P, Cornacchia G. Energy recovery from sugarcane-trash in the light of 2nd generation biofuels. Part 1: current situation and environmental aspects. Waste and Biomass Valorization. 2011;2(1):1-16.
5. Chindaprasirt P, Rattanasak U. Eco-production of silica from sugarcane bagasse ash for use as a photochromic pigment filler. Scientific Reports. 2020;10(1):9890.
6. Oliveira R, Mateus M, Santos D. Chronoamperometric and chronopotentiometric investigation of Kraft black liquor. International Journal of Hydrogen Energy. 2018;43(35):16817-23.
7. Parpot P, Bettencourt A, Carvalho A, Belgsir E. Biomass conversion: attempted electrooxidation of lignin for vanillin production. Journal of applied electrochemistry. 2000;30:727-31.
8. Parpot P, Servat K, Bettencourt A, Huser H, Kokoh K. TEMPO mediated oxidation of carbohydrates using electrochemical methods. Cellulose. 2010;17:815-24.
9. Sugano Y, Vestergaard Md, Yoshikawa H, Saito M, Tamiya E. Direct Electrochemical Oxidation of Cellulose: A Cellulose-Based Fuel Cell System. Electroanalysis. 2010;22(15):1688-94.
10. Yang F, Zhang Q, Fan H-X, Li Y, Li G. Electrochemical control of the conversion of cellulose oligosaccharides into glucose. Journal of Industrial and Engineering Chemistry. 2014;20(5):3487-92.
11. Sugano Y, Latonen RM, Akieh-Pirkanniemi M, Bobacka J, Ivaska A. Electrocatalytic oxidation of cellulose at a gold electrode. ChemSusChem. 2014;7(8):2240-7.
12. Sugano Y, Saloranta T, Bobacka J, Ivaska A. Electro-catalytic oxidation of hemicelluloses at the Au electrode. Physical Chemistry Chemical Physics. 2015;17(17):11609-14.
13. Movil O, Garlock M, Staser JA. Non-precious metal nanoparticle electrocatalysts for electrochemical modification of lignin for low-energy and cost-effective production of hydrogen. International Journal of Hydrogen Energy. 2015;40(13):4519-30.
14. Sugano Y, Kumar N, Peurla M, Roine J, Aho A, Bobacka J, et al. Specific electrocatalytic oxidation of cellulose at carbon electrodes modified by gold nanoparticles. ChemCatChem. 2016;8(14):2401-5.
15. Xiao H, Wu M, Zhao G. Electrocatalytic oxidation of cellulose to gluconate on carbon aerogel supported gold nanoparticles anode in alkaline medium. Catalysts. 2015;6(1):5.
16. Hibino T, Kobayashi K, Nagao M, Teranishi S. Hydrogen production by direct lignin electrolysis at intermediate temperatures. ChemElectroChem. 2017;4(12):3032-6.
17. Caravaca A, Garcia-Lorefice WE, Gil S, de Lucas-Consuegra A, Vernoux P. Towards a sustainable technology for H2 production: Direct lignin electrolysis in a continuous-flow Polymer Electrolyte Membrane reactor. Electrochemistry Communications. 2019;100:43-7.
18. Hibino T, Kobayashi K, Lv P, Nagao M, Teranishi S. High performance anode for direct cellulosic biomass fuel cells operating at intermediate temperatures. Bulletin of the Chemical Society of Japan. 2017;90(9):1017-26.
19. Rafiee M, Alherech M, Karlen SD, Stahl SS. Electrochemical aminoxyl-mediated oxidation of primary alcohols in lignin to carboxylic acids: Polymer modification and depolymerization. Journal of the American Chemical Society. 2019;141(38):15266-76.
20. Li S, Song X. Study on the preparation and production factors of a direct lignocellulose biomass fuel cell. Journal of Electroanalytical Chemistry. 2018;810:55-61.

21. Muiuane V, Ferreira M, Bignet P, Bettencourt A, Parpot P. Production of formic acid from biomass-based compounds using a filter press type electrolyzer. Journal of Environmental Chemical Engineering. 2013;1(4):1237-44.
22. Harrison KW, Remick R, Hoskin A, Martin G. Hydrogen production: fundamentals and case study summaries. National Renewable Energy Lab.(NREL), Golden, CO (United States); 2010.
23. Raeva V, Gromova O. Separation of water–formic acid–acetic acid mixtures in the presence of sulfolane. Fine Chemical Technologies. 2019;14(4):24-32.